ADVANCED ENERGY MATERIALS
www.advenergymat.de

Materials Views
www.MaterialsViews.com

# Domain Purity, Miscibility, and Molecular Orientation at Donor/Acceptor Interfaces in High Performance Organic Solar Cells: Paths to Further Improvement

*Wei Ma, John R. Tumbleston, Ming Wang, Eliot Gann, Fei Huang, and Harald Ade**

**Domain purity and interface structure are known to be critical for fullerene-based bulk heterojunction (BHJ) solar cells, yet have been very difficult to study. Using novel soft X-ray tools, we delineate the importance of these parameters by comparing high performance cells based on a novel naphtha[1,2-c:5,6-c]bis[1,2,5]thiadiazole (NT) material to cells based on a 2,1,3-benzothiadiazole (BT) analogue. BT-based devices exhibit ~15 nm, mixed domains that differ in composition by at most 22%, causing substantial bimolecular recombination. In contrast, NT-based devices have more pure domains that are >80 nm in size, yet the polymer-rich phase still contains at least 22% fullerene. Power conversion efficiency >6% is achieved for NT devices despite a domain size much larger than the nominal exciton diffusion length due to a favourable trade-off in the mixed domain between exciton harvesting, charge transport, and bimolecular recombination. The miscibility of the fullerene with the NT and BT polymer is measured and correlated to the purity in devices. Importantly, polarized x-ray scattering reveals preferential face-on orientation of the NT polymer relative to the PCBM-rich domains. Such ordering has previously not been observed in fullerene-based solar cells and is shown here to be possibly a controlling or contributing factor to high performance.**

## 1. Introduction

Although it is recognized that the morphology of a high efficiency bulk heterojunction solar cell[1–6] is critical to its performance, quantitative measurements of the domain purity, domain size and the nature of the interface structure are often lacking. Even within the canonical paradigm of small domains on the order of the exciton diffusion length of~10 nm, the purity of the two phases has not been considered in detail until recent studies of miscibility and bilayer interdiffusion indicated that amorphous domains in poly(3-hexylthiophene) (P3HT) are not pure, leading to the discussion of three or even four phases in some systems.[7–15] The likelihood of impure domains prompted other important questions relating to the nature of the donor/acceptor interface such as differences in interface structure, which could also influence device performance.

Direct measurements of domain purity in actual devices have not been achieved yet in most systems, due to a paucity of suitable characterization methods. Common real space methods such as scanning probe microscopy and transmission electron microscopy (TEM) elucidate the morphology only qualitatively. Energy filtered TEM has been used to achieve enhanced compositional contrast,[11,16–18] but quantification of domain composition is still difficult. X-ray microscopy has also been successfully used in a number of systems that have large enough domains to quantify the composition. However, the spatial resolution is limited to ~50 nm and the complex modulation transfer function only provides upper composition limits in many cases.[19–21] In terms of reciprocal space methods, studies using resonant soft X-ray Scattering (R-SoXS) have successfully quantified domain purity and domain size by considering the total scattering intensity and the location of scattering peaks, respectively.[22,23] For the high performing blend based on poly[[4,8-bis[(2-ethylhexyl)oxy]benzo[1,2-b:4,5-b′]dithiophene-2,6-diyl][3-fluoro-2-[(2-ethylhexyl) carbonyl]thieno[3,4-b] thiophenediyl]] (PTB7) and [6,6]-phenyl C71 butyric acid methyl ester ($PC_{71}BM$), the combination of R-SoXS with x-ray microscopy showed that the active layer consists of a PCBM pure phase dispersed in a modestly impure polymer-rich matrix comprised of ~30% PCBM.[23] For very low purity, i.e. high levels of mixing, it has been argued that significant charge recombination occurs,[24] which is consistent with Monte-Carlo simulations.[25] On the other hand, if domain purity is too high and domains are too large, it is also possible that charge percolation pathways to the electrodes are lost, leading to a worsening of device performance.[26] These studies reveal that domain purity may have a "sweet spot" in many systems that yield maximized

Dr. W. Ma, Dr. J. R. Tumbleston, E. Gann, Prof. H. Ade
Department of Physics
North Carolina State University
Raleigh, NC 27695, USA
E-mail; harald_ade@ncsu.edu
Dr. M. Wang, Prof. F. Huang
Institute of Polymer Optoelectronic Materials & Devices
State Key Laboratory of Luminescent Materials and Devices
South China University of Technology
Guangzhou 510640, P. R. China

DOI: 10.1002/aenm.201200912

performance. More fundamentally, it remains unclear how differences in purity between domains in devices based on different materials are linked to fundamental thermodynamic properties, such as molecular miscibility, and if such properties can be used to predict morphology and thus performance.

The structure of the heterojuction in polymer:fullerene blends is even less studied than domain purity. It has been shown experimentally in diketopyrrolopyrrole (DPP) based polymer PDPP3T cast from ternary solvents, model polymer/polymer bilayers and through Monte-Carlo simulations and polymer/polymer bilayer studies that roughness of the interface decreases performance.[25,27,28] The interface structure of P3HT:PCBM has also been characterized in thick films, but not linked to device performance.[9] In the high performance system PTB7:$PC_{71}BM$, scattering analysis revealed a slightly diffuse interface in films cast without DIO.[23] Besides interface roughness, molecular ordering and orientation at the donor/acceptor interface is likely critical, but has not yet been delineated in BHJ devices. In small-molecule bilayer devices and polymer-polymer systems, interfacial ordering and preferential orientation has been suggested to be important and in the case of a phthalocyanine/C60 interface, face-on orientation was shown to correlate with better performance.[29–32] However, this potentially critical parameter has yet to be observed and investigated in polymer/fullerene blends with non-planar donor/acceptor heterojunctions that are distributed throughout the active layer.

In this work, we measure the domain purity and interface structure of blends based on two novel polymers recently developed by Wang *et al*.[33] These polymers are identical but for one difference; the novel naphtha[1,2-c:5,6-c]bis[1,2,5]thiadiazole (NT) is replaced by the widely used 2,1,3-benzothiadiazole (BT) moiety (chemical structure shown in **Figure 1**). PBDT-DTNT blends with either $PC_{61}BM$ or $PC_{71}BM$, referred to as NT:61 and NT:71 hereafter, result in power conversion efficiency (PCE) of up to ~6.1% without any special interface contact engineering, values five times higher than for the BT:61 and BT:71 counterpart devices. We show that the differences between NT and BT devices are in-part due to significant differences in bimolecular recombination in the active layer. Utilizing R-SoXS,[34–36] the domain purity is shown to be much lower and the domain size much smaller for BT than NT-based devices. NT:71 devices perform surprisingly well given their large domain size of ~80 nm. Utilizing near edge X-ray absorption fine structure (NEXAFS) spectra of annealed mixtures and fitting it with pure reference spectra, the measured miscibility[8,37] of $PC_{61}BM$ and $PC_{71}BM$ with BT and NT is shown to be a fundamental, thermodynamic driver that can explain broadly the observed differences in purity and the need for only mild annealing protocols used for NT devices.[33,38] The crystallization behaviour of the BT and NT devices revealed by Grazing Incidence Wide-Angle X-ray Scattering (GIWAXS) is linked to the purity of the domains and miscibility. In terms of interface properties, polarized soft x-ray scattering[29] demonstrates molecular orientational ordering relative to the BHJ interface in the active layer. It is found that preferential face-on molecular orientation occurs for NT-based devices, whereas BT devices show random orientation.

The combination of characterization methods used here results in a comprehensive picture of the morphology, which in turn explains the device performance for BT- and NT-based devices, and delineates the impact the various morphological parameters have. Use of common qualitative morphological characterization tools would have been inadequate to elucidate device performance. Ultimately, our results highlight that detailed characterization of domain purity, domain spacing, miscibility, and molecular ordering at the D/A interface are required in order to fully understand the correlations between morphology, chemical structure, thermodynamic properties, and performance of OPV devices. At the same time, we explain the performance of devices based on two novel, recently introduced materials,[33] one of which, NT, is very promising and has shown excellent performance with a PCE of 8.4% when used in an inverted structure with a ~250 nm thick active layer and with an electron-extracting, polyelectrolyte interlayer.[38] Based on our incident photon-to-current efficiency (IPCE), light intensity measurements, morphological characterization, and optical considerations, further improvement for the NT:71 system should be possible with better control of the morphology.

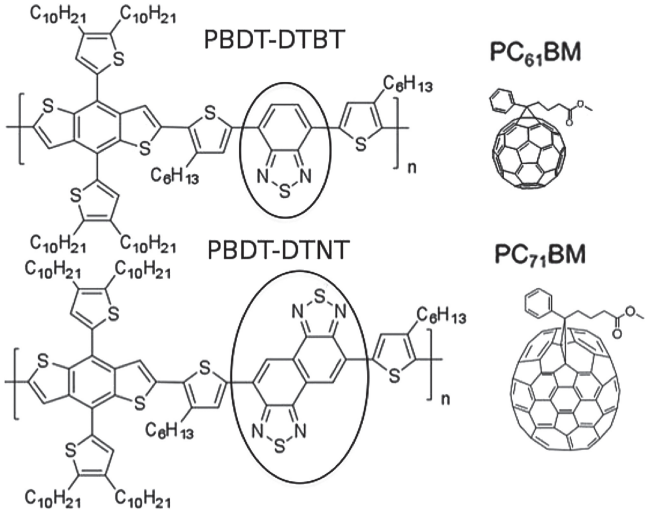


**Figure 1.** Chemical structures of polymers, BT and NT, with BT and NT units circled. Chemical structures of fullerenes used herein, $PC_{61}BM$ and $PC_{71}BM$, are also shown.

## 2. Results and Discussion

### 2.1. Device Performance and Bimolecular Recombination

Solar cells were fabricated following previously established protocols for these materials[33] by spin-coating BT and NT mixed with either $PC_{61}BM$ or $PC_{71}BM$ (see Experimental Section for fabrication details. We note here that BT and NT have similar molecular weight and polydispersity indices.) Current density vs voltage (J-V) curves of the resulting devices are presented in **Figure 2**(a) and device characteristics are displayed in **Table 1**, where nearly identical performance to Wang et al,[33] is achieved. BT:71 and NT:71 exhibit considerably higher PCE than their BT:61 and NT:61 counterparts, with the highest PCE = 6.14% achieved for NT:71 devices ($J_{sc}$ = 13.2 mA/cm$^2$, $V_{oc}$ = 0.79 V, FF = 0.59). Regardless of polymer, $J_{sc}$ is enhanced and $V_{oc}$ and FF are almost identical

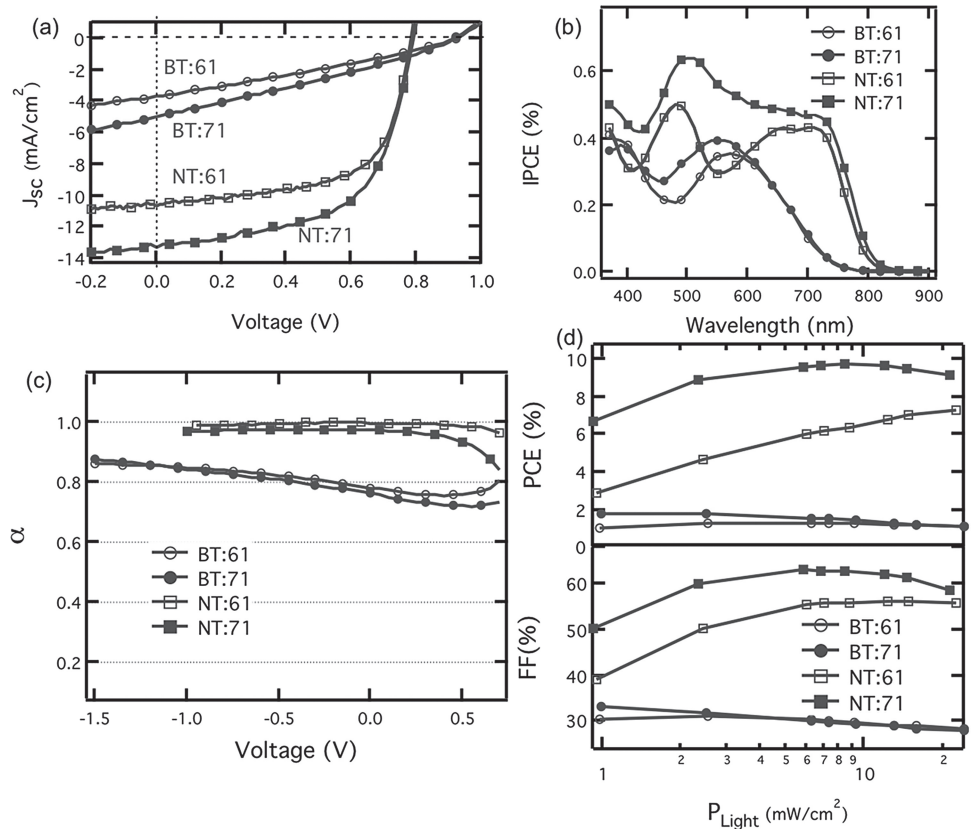


**Figure 2.** Device charactristics for BT:61, BT:71, NT:61 and NT:71: (a) Current-voltage characteristics under 1-sun illumination; (b) Incident-photon-to-current efficiency (IPCE) spectra of different devices; (c) Scaling exponent, $\alpha$, of photocurrent with light intensity for different devices and (d) Fill factor (FF) and power conversion efficiency (PCE) measured from data used to determine Figure 2(c).

when using $PC_{71}BM$ compared to $PC_{61}BM$. This is due in part to stronger absorption of $PC_{71}BM$ compared to $PC_{61}BM$,[33] which is in agreement with the IPCE data shown in Figure 2(b).

Significantly higher $J_{sc}$ and FF values are observed for NT-based devices than for BT devices. One reason for higher $J_{sc}$ is due to the broader absorption range for NT-based blends as evidenced from the extended IPCE further into the near-IR (see Figure 2b). However, this does not fully explain the differences in $J_{sc}$ since the FF is around two times higher for NT devices, indicating that high recombination levels also limit $J_{sc}$ for BT-based solar cells. In order to investigate differences in recombination, the power-law scaling of the photocurrent ($J_{photo} = J_{light} - J_{dark}$) with laser light intensity ($\lambda$ = 632 nm) is measured to probe bimolecular recombination.[39,40]

$$J_{photo} = \beta \left(P_{light}\right)^{\alpha}$$

**Table 1.** Photovoltaic data of the BT, NT based polymer with $PC_{61}BM$ and $PC_{71}BM$.

| Active layer | $J_{sc}$ (mA/cm$^2$) | $V_{oc}$ (V) | FF | PCE (%) |
|---|---|---|---|---|
| BT:61 | 3.65 ± 0.08 | 0.93 ± 0.01 | 0.30 ± 0.01 | 1.02 ± 0.10 |
| BT:71 | 5.08 ± 0.08 | 0.93 ± 0.01 | 0.29 ± 0.01 | 1.37 ± 0.09 |
| NT:61 | 10.61 ± 0.09 | 0.78 ± 0.01 | 0.62 ± 0.02 | 5.13 ± 0.10 |
| NT:71 | 13.23 ± 0.08 | 0.79 ± 0.01 | 0.59 ± 0.02 | 6.14 ± 0.10 |

where $J_{photo}$ is the photocurrent, $\beta$ is a constant, $P_{light}$ is light intensity and $\alpha$ is the scaling exponent. Briefly, when the light intensity is increased, electron and hole concentrations also increase and trigger bimolecular recombination if carriers are not able to exit the active layer. For $\alpha \approx 1$, bimolecular recombination is minimal. On the other hand, stronger bimolecular recombination will lead to a sublinear dependence of $J_{photo}$ with $P_{light}$ and a correspondingly lower $\alpha$ value. Figure 2(c) shows $\alpha$ as a function of applied voltage where $\alpha \approx 1$ is observed for NT-based blend films, except for voltages near $V_{oc}$ for the NT-71 devices. This suggests that few free carriers are lost due to bimolecular recombination. However, for BT-based blend films, maximum power point is reached at an applied voltage of ~0.6 V. At this voltage, $\alpha$ is ~0.75, which implies space charge limited photocurrent.[41] Since $\alpha$ for BT-based devices are much less than those based on NT over the entire applied voltage range, bimolecular recombination is much stronger for solar cells based on BT. This causes a reduction in not only the FF where the internal electric field in the active layer is relatively low, but even under short-circuit conditions which helps explain the lower $J_{sc}$ for BT-based devices. Differences in bimolecular recombination are supported by corresponding FF and PCE measurements under variable light intensity (Figure 2(d)). Significant differences in FF, $J_{sc}$ and PCE between BT and NT-based devices are observed for light intensities ranging from 1 to 25 mW/cm$^2$ ($J_{sc}$ is plotted in Supporting Information). The FF for BT-based solar cells monotoni-

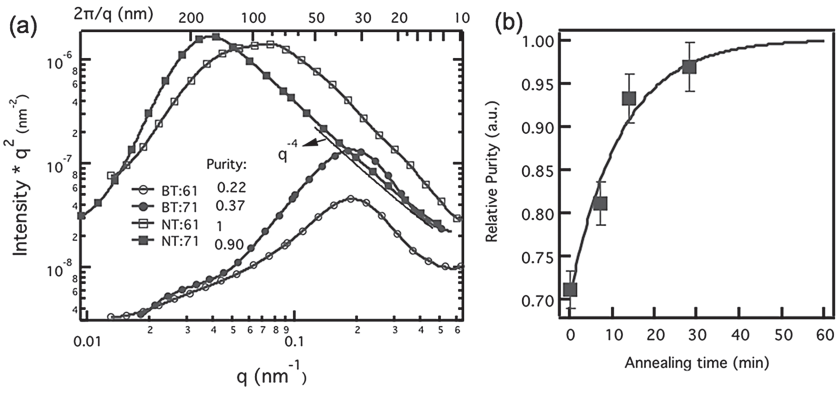


**Figure 3.** (a) R-SoXS scattering profiles (284.1 eV) of blend films of BT:61, BT:71, NT:61 and NT:71 (as indicated) annealed at 130 °C for 7 min. TSI values of 0.05, 0.14, 1, 0.81 (corresponding relative domain purities are 0.22, 0.37, 1 and 0.9 calculated from square root of TSI) for BT:61, BT:71, NT:61 and NT:71, respectively. The high-q scaling of –4 for NT:71 reveals a sharp interface. (b) Relative purities of NT:71 blend as a function of annealing time at 130 °C.

cally decreases with increasing light intensity, while devices with NT polymers peak in FF for higher light intensities. Along with the scaling exponent, this supports that bimolecular recombination is much stronger for BT- compared to NT-based solar cells.

### 2.2. Domain Size and Purity

The differences in device performance depending on the use of BT or NT are dramatic, with significant bimolecular recombination loss in BT-based devices. It is presumed that these differences are at least in part due to morphological variations since the chemical structures of the conjugated polymers are not exceedingly different. In order to probe the dominant length scales of the morphology and relative purity between polymer-rich and fullerene-rich domains, R-SoXS is utilized.[34–36] A photon energy of 284.1 eV is selected to provide high polymer/fullerene contrast while avoiding high absorption associated with the carbon 1s core level, which would produce background fluorescence and can lead to radiation damage.[42] The contrast functions of polymer/fullerene, polymer/vacuum and fullerene/vacuum near the carbon 1s absorption edge are displayed in Figure S1. Furthermore, using 284.1 eV photons has the advantage that the contrast between polymer and fullerene is not sensitive to the fullerene type. **Figure 3**(a) shows the scattering profiles acquired for the four blends investigated. We observe similar relative distributions of domain size for NT:fullerene and BT:fullerene blends, respectively. In contrast, the domain size varies considerably when comparing blends based on the different polymers. A dominant domain spacing of 84 and 160 nm is observed for NT:61 and NT:71, respectively, while a spacing of ~30 nm is found for both BT-based blends. Scanning transmission X-ray microscopy (STXM) measurements confirm the domain spacing of NT:71 blend films (see Supporting Information Figure S2) for which a semi-bicontinuous morphology is observed.

Along with the distribution of domain spacings, the relative domain purity is also extracted from R-SoXS measurements. This is achieved by calculating the total scattering intensity (TSI) via integration of the scattering profiles over the q-range measured (See Supporting Information) and conversion to purity.[23] The TSI measures the average sample composition fluctuations. Relative purities, assuming a two-phase model and averaged over the size scales probed with R-SoXS, of 0.22 and 0.37 are obtained for BT:61 and BT:71, and 1 and 0.90 for NT:61 and NT:71, respectively. NT-based devices have domains that are thus much purer than BT-based devices. The two phases in the BT:61 and BT:71 device (with a relative purity of 0.22 and 0.37) differ in composition from each other by at most 22% and 37%. This upper limit can be deduced by assuming that the relative purity of NT:61 actually does correspond to 100% pure domains. In reality, the purity of NT:61 is less than 100% due to fundamental limits imposed by the miscibility of the fullerene in the polymer (see below), which further reduces the composition differences of the two phases in the devices. Relatively impure domains have been previously cited to lead to bimolecular recombination in other systems.[43,44] This can be readily understood as highly mixed systems do not have good charge transport pathways, i.e. exhibit low mobility, and high number of trap states, both of which lead in a compounding way to poor performance. The light intensity measurements shown in Figure 2 are thus readily explained by the purity of the domains and explain, at least partly, why NT-based blend films have much higher FF (~60%) than BT-based blend films (~30%). Interestingly, we note that the domain size in the best devices (i.e., those based on NT) is much larger than for BT-based blend, even though traditionally it is thought that smaller domain size (near 10 nm)[45–47] is favourable for exciton diffusion to donor/acceptor interfaces. The impure domains of devices comprised of BT clearly negate the nominal relative advantage of the small size.[28] We note that the most efficient device, NT:71 (PCE = 6.1%), shows the largest domain size. Even so, only 50–60% IPCE is achieved (Figure 2b), which indicates that NT:71 devices still have room for further efficiency improvements. NT:71 devices with 8.4% PCE yet comparable FF of ~0.60 employed ~250 nm thick active layers[38] compared to the ~90 nm active layers used in this and previous work.[33] Much of the improvement in $J_{sc}$ relative to prior devices is thus likely due to increased absorption. Consequently, use of processing protocols that reduce the domain size and optimize the purity are likely to further enhance the current output and improve FF.

The purer domains of the NT:61 relative to the NT:71 device also correlate with the reduced bimolecular recombination (near $V_{oc}$) and higher FF observed for the NT:61 devices. However, in contrast to the NT devices, the BT:61 and BT:71 devices exhibit only small differences in $\alpha$ and FF (See Figure 2), yet BT:71 has domains that are more pure than those in BT:61 by a factor of 0.37/0.22 = 1.7. Near the limit of completely mixed domains, one would expect that purer domains perform better. Hence, an apparent contradiction emerges as a 1.7 times difference in purity leads to essentially the same performance.

One possible resolution of this situation might be that there is a fundamental difference in the bimolecular recombination coefficient that depends on the fullerene: The better molecular level performance of BT:61 overcomes the higher mixing of the domains in this system. However, in order to come to firm conclusions, the relative difference in absorption, i.e. a complete optical model, and possible consideration of other parameters is required. A full analysis of this aspect is outside the scope of this paper. We note though that the observed apparent contradiction is intriguing and that the extraction of a molecular level recombination coefficient is only possible if quantitative purity as provided here is measured.

Pure domains should lend themselves more readily to be crystalline, or visa versa, crystalline or molecularly ordered domains should lead to relatively pure domains. It is thus not entirely surprising that crystallinity has previously been cited to play a role in performance,[11,48,49] although several studies have also reported that crystallinity did not necessarily improve devices.[50,51] Grazing incidence wide angle x-ray scattering (GI-WAXS) was nonetheless used as a complementary tool to characterize the crystalline nature of BT and NT neat polymers and their blends with $PC_{61}BM$ and $PC_{71}BM$ (see Figure S3). For BT based blend films, a slight (100) peak but no (010) peak are observed, indicating that BT based films are rather amorphous. For NT based blend films, although some lamellar (100) and face-on (010) intensity is observed, a broad peak distribution and rapid disappearance of the (200) and lack of (300) higher-order peaks signifies that NT has relative short–range order and is not highly crystalline. In order to analyze the degree of molecular order, the paracrystallinity parameter, g,[52] has been calculated from the (010) $\pi$–$\pi$ stacking peak, yielding g = 10.5% and g = 10.6% for NT:71 and NT:61 blend films, respectively (see Figure S4). These g values are close to the value of amorphous silicon dioxide ($SiO_2$) glass, which has g = 12%.[52] This suggests that the NT polymer forms disordered aggregates and not polymer crystals.[26] We note that with a g value this high, one cannot associate a defined grain size with the ordering, which is consistent with the fact that no separate feature is observed with R-SoXS at the corresponding grain size at high q. Rather, the high q data for NT:71 displays a relatively well defined scaling relation with a slope close to $q^{-4}$. This indicates that the polymer/fullerene interface is rather sharp and that except for the ~80 nm domains, there is no other important length scale in these devices that exhibits compositional contrast. The improved local ordering observed with GI-WAXS simply correlates with the higher purity polymer domains of the NT polymer, but does not lead to any well-developed structures with a particular length scale. In addition to increased local ordering, NT shows some preferential face-on orientation with respect to the substrate, which in some previous studies was thought to benefit device performance.[53,54] However, edge-on orientation occurs for P3HT where high FF is achieved.[12] Consequently, it is difficult to directly link GI-WAXS derived parameters to the device performance of this system. We find the impact of domain purity on device performance is more pronounced and more direct in the systems discussed here.

While the relative purity values from R-SoXS are related to crystallinity, the absolute composition cannot be obtained at the present time from single R-SoXS measurements due to a lack of sufficient absolute flux normalization. To obtain a sense of the absolute domain purity of these blends, a series of NT:71 blend films were annealed at 130 °C for a range of times and subsequently measured with R-SoXS. The relative domain purity is plotted in Figure 3(b) and demonstrates that the purity increases with further annealing and approaches a saturated value as expected. For the 7 min annealed sample that corresponds to the devices characterized, the purity is at most ~82% of the saturated purity value of the longer annealed samples. This demonstrates that the domains of the NT-based devices have not yet completely purified. While these purities are still relative, the upper limit of absolute domain purity is given by the miscibility of fullerene in the polymer. This will be discussed in the next section.

### 2.4. Molecular Miscibility

Fundamentally, thermodynamic properties of donor and acceptor, i.e. molecular miscibility, provide the driving force of the mixture between donor and acceptor materials to phase separate, thus controlling the morphology formation and impacting recombination processes in BHJ organic solar cells.[8,13,37] Practically, the thermodynamic miscibility also represents an upper limit of domain purity in the blend films as discussed below. The lower purity of BT-based blends compared to those comprised of NT as observed with R-SoXS, implies that the driving force for phase separation during thermal annealing is lower for BT-based blends implying that fullerenes have a higher molecular miscibility with BT than with NT. This is supported by directly measuring the miscibility of the fullerene with the polymer using previously established protocols.[21] Near edge X-ray absorption fine structure (NEXAFS) spectra were acquired of molecularly mixed regions of films that had been thermally annealed for 48 h at 190 °C to reach local equilibrium and complete phase separation. At equilibrium, PCBM forms large crystals up to hundreds of microns in size as observed by visible light microscopy and STXM (see Supporting Information Figure S5). The blend ratios (polymer:fullerene by weight) required to induce complete phase separation at 190 °C were 1:1 for NT-based blends and 1:2 for BT-based blends. The higher fullerene concentration needed for BT-based blends implies higher miscibility of fullerene with BT. NEXAFS spectra near the carbon 1s absorption edge acquired between large PCBM crystals (see Supporting Information Figure S5) confirm this conjecture. **Figure 4** represents the NEXAFS of the aggressively annealed NT and BT-based blends films with either $PC_{61}BM$ or $PC_{71}BM$. These NEXAFS spectra were fitted using pure component reference spectra for the respective polymer and fullerene (black dot and grey solid curves).[8,37] The resulting fullerene miscibility with BT is 23.1(7)% (fullerene weight percentage) for $PC_{61}BM$ and 35.6(8)% for $PC_{71}BM$, respectively. Extremely low miscibilities of 3.1(7)% and 5.0(1)% compared to prior miscibility measurements[8,21,37,55] were extracted for $PC_{61}BM$ and $PC_{71}BM$ in NT, respectively. We note that the miscibility of $PC_{61}BM$ is smaller than that of $PC_{71}BM$ for both polymers, a trend similar to that observed for other semi-conducting polymers.[37,55] We note that the molecular weights and polydispersity of the NT

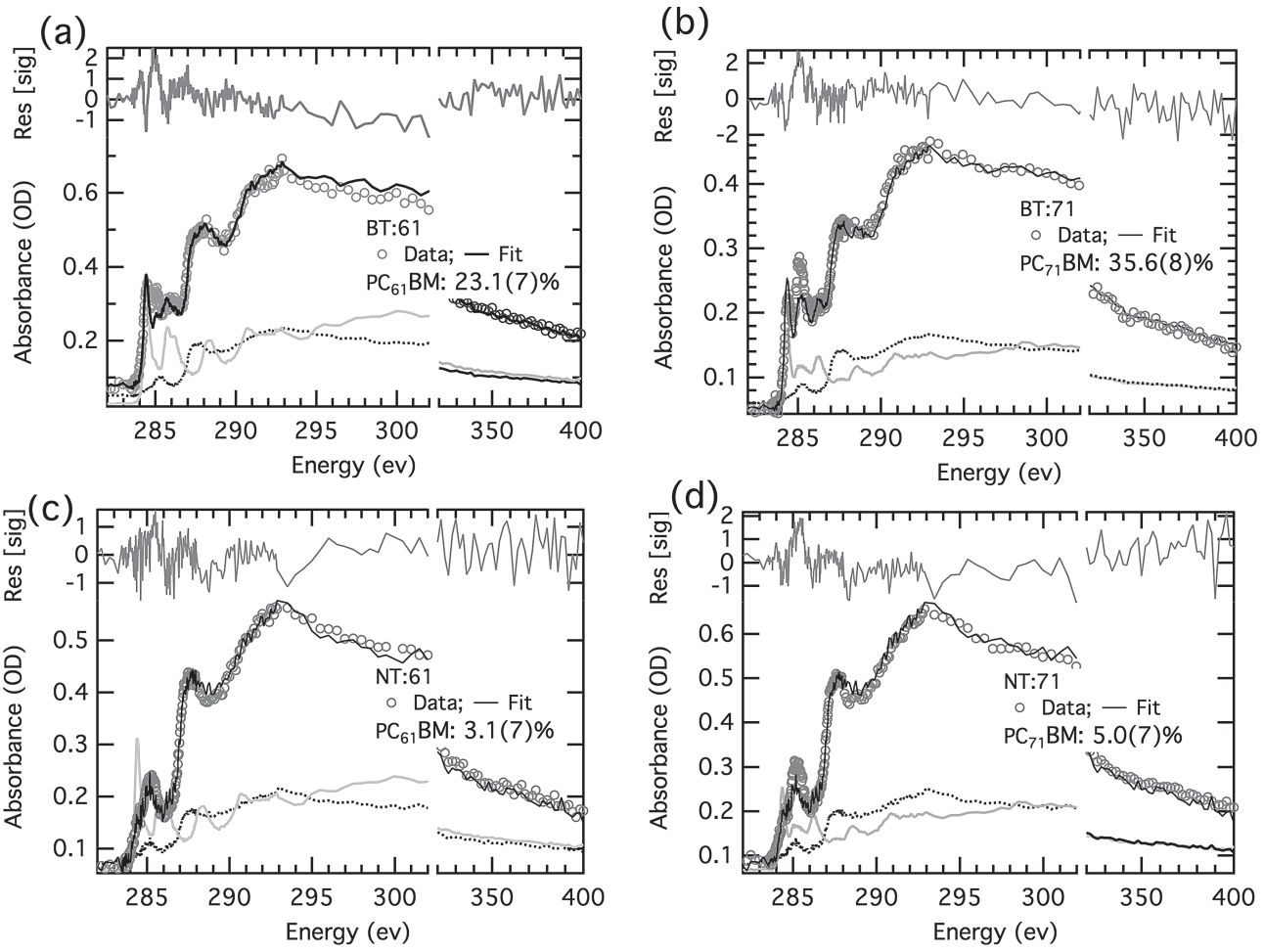


**Figure 4.** NEXAFS spetra and fits of the residual matrix of polymer:fullerene blend films annealed for 48 h at 190 °C: (a) BT:61; (b) BT:71 ; (c) NT:61 and (d) NT:71. Black dot and grey solid line are the NEXAFS of polymer and fullerene reference films, respectively.

and BT polymer are rather similar and that the differences in miscibility have to be enthalpic in character and must relate to the structural differences of the backbone. Concerning device morphology and thus recombination mechanisms, a lower miscibility should induce the development of purer domains, which limit bimolecular recombination, thereby increasing FF. From the evidence outlined above, the relative domain purity between NT and BT correlates overall with the miscibility of the fullerenes in these polymers, and the thermodynamic miscibility might thus be used as a measure to predict device morphology and performance. However, subtle differences exist from a simple predictive model based on polymer/fullerene miscibility alone. BT:71 has purer domains than BT:61, even though the miscibility of $PC_{61}BM$ is lower in BT than that of $PC_{71}BM$. We note that annealing sequences for NT:71 blend films showed that domains do not coarsen during annealing, but only purify. The overall domain size is thus set during casting/drying of the film and the miscibility and solubility in the solvent used for casting, i.e. the ternary phase diagram, as well as kinetic factors that depend on the solvent boiling point. Nonetheless, the relative miscibility predicts the overall morphology and performance between polymers.

Finally, we return to the composition of the NT:71 devices assuming a two phase morphology. Combining the annealing sequence and miscibility measurement, we estimate the upper limit of the absolute domain purity as follows: Since the relative purity for devices is ~82% of the saturated value (Figure 3b), which can be no purer than the misciblity limit of ~5%, an upper limit of purity of at most 78% polymer and at least ~22% PCBM can be inferred for the polymer-rich domains in NT:71. Based on the relative purity of the NT:71 and NT:61 system of 1.0 and 0.9, respectively, we can also conclude that the polymer-rich domains of NT:61 are at most ~87% polymer. We note that domains with even higher purity might not be always beneficial as recently inferred by Bartelt et al.[26] Large domains that become too pure exhibit a lack of percolation pathways that leads to reduced device performance. Hence, by fine tuning domain size and purity, the device performance could be further improved, especially for NT:71 that achieved PCE = 6.1%. The very low miscibility of the NT-based blends furthermore explains and predicts why only mild annealing[33,38] for a few minutes at <130 °C is used, as the purity of the NT domains that are larger than the exciton diffusion length can become too high to provide efficient charge transport to the electrodes.

### 2.5. Heterojunction Characteristics: Orientational Ordering and Compositional Structure

While the compositional donor/acceptor heterojunction structure, i.e. sharpness, roughness or diffuseness, is revealed by analysing the slope of the scattering profile at high-q (Figure 3a), molecular ordering at the donor-acceptor interface might also be a critical structure parameter that impacts performance. This ordering may influence exciton dissociation at and charge transport near an interface. Regarding compositional structure, we focus here on the NT:71 system, as it exhibits the highest performance and the clearest scaling relation, with a scaling very close to $q^{-4}$. Such a scaling indicates that the interfaces between the polymer-rich and the $PC_{71}BM$ domains are very sharp and smooth. Regarding molecular ordering, Collins et al. recently discovered scattering anisotropy in polymer-polymer organic solar cells using polarized soft x-ray scattering (P-SoXS), a method which can probe crystalline and non-crystalline molecular orientation, and inferred a preferential face-on orientation of the matrix polymer with respect to the dispersed phase in a polymer:polymer blend.[29] No correlation to device performance had been established. In contrast, Rand et al. observed qualitatively that orientational ordering at the donor/acceptor interface impacts small-molecule, bilayer devices, where a face-on orientation is concluded to be more favourable for performance.[30,32] However, other previous studies on interfacial orientation had concluded that edge-on might be preferable.[31] Clearly, the structure of the D/A interface is critical and needs to be carefully characterized and correlated to performance. Here, we observe ordering for the first time in the most widely used and most efficient family of organic solar cells, polymer-fullerene BHJ devices. Interestingly, interfacial ordering was observed for both NT:61 and NT:71 blend films, but not for BT-based blend films. Ordering apparently depends strongly on the polymer species and their particular molecular design. **Figure 5**(a) shows P-SoXS profiles of NT:71 and BT:71 blend films integrated over 10° azimuthal sectors, where solid and dashed lines represent parallel and perpendicular sectors (relative to the polarization), respectively. At 285.1 eV, orientation sensitivity is enhanced, and thus significant differences between parallel and perpendicular profiles are observed. This anisotropy is caused by preferential face-on orientation at the donor/acceptor interface, following the arguments delineated by Collins et al.[29] The molecular orientation and alignment is schematically depicted in Figure 5(b). Such molecular orientation should promote overlap of the $\pi$ orbital with the PCBM phase and promote exciton dissociation and thus higher device performance.[30] $\pi$–$\pi$ stacking in the direction normal to the interface, even if imperfect, should also promote better charge transport away from the interface in complete analogy to the effect of face-on crystallite orientation relative to the electrodes. However, as discussed above, the $\pi$–$\pi$ stacking is not very pronounced. Scattering anisotropy is not observed in BT-based blends, indicating that BT is randomly oriented with respect to the BHJ donor/acceptor interfaces. The BT interfaces do not exhibit any clear scaling relation and are thus unlikely to be sharp or exhibiting a well defined structure. Relatively abrupt and smooth interfaces such as those exhibited by NT:71 might thus be required to promote molecular ordering at these interfaces. Alternatively, agglomeration in the solution might be a confounding factor controlling both the sharpness and the molecular orientation of the D/A interfaces in the active layer of a device. Overall, the molecular ordering of the polymer must arise from differential interactions of the backbone and the side-chains with the fullerene that favors a face-on rather than edge-on orientation.

Our observations demonstrate that molecular orientational ordering as revealed by scattering anisotropy with P-SoXS also correlates with device performance and is therefore an important structure parameter that needs to be characterized and considered alongside others in order to understand high performance in organic solar cells. It might also be a parameter that should be considered alongside miscibility when designing new materials. To date, most considerations about new materials focus on controlling the electronic structure. Although it is difficult to predict physical structure based on molecular design, increasing effort needs to be paid to that in the future. Ideally, at least a rule-of-thumb, if not fully predictive models, need to be developed for an increased rational approach to progress.

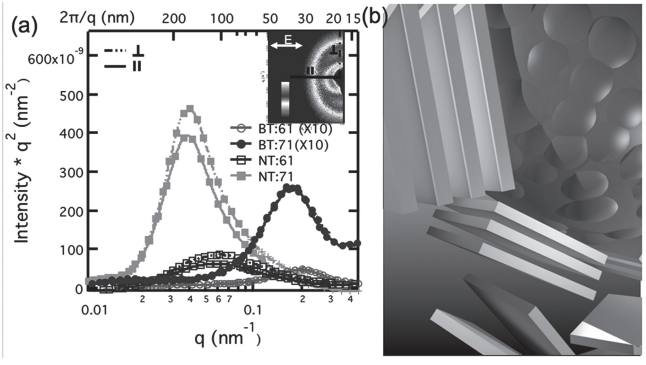


**Figure 5.** (a) Radial anisotropic scattering profiles of BT:61 (×10), BT:71 (×10), NT:61 and NT:71 obtained with a photon energy of 285.1 eV. Dash lines and solid lines represent data average over 10° azimuthal sectors perpendicular and parallel to the photon polarization, respectively. The inset shows 2D scattering data acquired with horizontally polarized x-rays. (b) Schematic of face-on molecular orientational ordering of NT polymers (white planes) with respect to $PC_{71}BM$-rich domains (dark regions).

## 3. Conclusion

We have shown that the domain purity, domain size and the nature of the interface structure in BHJ organic solar cells are critical for their performance and provide for the first time a quantitative comparison of domain purity between devices based on polymers with a different backbone. Interestingly, it is found that NT-based devices have larger and purer domains than BT-based devices. However, the purity of the polymer-rich, >80 nm domains in the high performance NT-based devices is at most 78% polymer. This suggests that domain purity plays an important role in determining device performance and that an acceptable balance between exciton dissociation, transport, and transport length scale (i.e. domain size) can be struck to yield high performance even if the domains are much larger than the nominal exciton diffusion length. Small and pure

domains might perform better yet, but a process needs to be devised to achieve that. The purity differences of the devices are consistent with fullerene miscibility measurements in the polymers, which reveals that NT-based polymers yield much lower fullerene:polymer miscibility than BT-based polymers. Miscibility and the propensity for short range order provide the driving force, or lack thereof, for the thin films to evolve towards relatively pure domains. Hence, miscibility of the fullerene in the polymer can thus be used as a guiding principle for the design of good devices, and very high miscibility should be avoided as it leads to domains that are too mixed and impure. Conversely, very low miscibility predicts relatively pure domains, where overannealing can lead to purification that is too high and therefore detrimental if domains are larger than the exciton diffusion length. Finally, molecular orientational ordering at the donor-acceptor heterojunction interface is revealed in NT-based polymer blends through scattering anisotropy, which is an additional parameter that can control device performance. Our results illustrate that domain purity and molecular orientational ordering should be widely considered when explaining high performance devices. They also reveal that reduction of domain size and fine tuning of the purity and domain interface structure should lead to improved NT-based solar cells. For thicker films, a PCE above 9% seems possible.

Overall, a more subtle picture of the BHJ paradigm of solar cell operation emerges. The canonical picture that pure domains ~10 nm in size are needed for best performance is expanded to include morphologies that still yield excellent performance and exhibit large domains with sufficient mixing to provide percolation for charges, but pure enough to avoid excessive bimolecular recombination. Furthermore, interfacial structure is emerging as an important aspect of polymer:fullerene devices that warrants further investigations. In order to disentangle the relative importance of purity, size, and molecular ordering, more extensive studies manipulating these parameters are required. Clearly, without measurement of the morphological parameters described here, it is difficult to make definitive conclusions about the importance of any one parameter for the device performance. A complete morphological analysis will likely unravel the critical structure-performance relationships in many OPV systems.

## 4. Experimental Section

*Samples*: The synthesis method of BT and NT polymers is presented in reference.[33] In this batch, Mn of BT is 25.8 K with PDI = 2.45; Mn of NT is 36.1 K with PDI = 2.05. $PC_{61}BM$ and $PC_{71}BM$ are purchased from Nano-C. Blend films for devices, x-ray scattering and x-ray absorption were prepared using an identical procedure to Wang et al.[33]

*Device fabrication*: Devices were fabricated by spin-coating blend solutions on PEDOT:PSS–coated (~40 nm) indium-tin-oxide ITO glass substrates and then annealing in air at 120 °C for 15 min. Blend solutions of polymer:fullerene were prepared from 1,2-dicholorobenzene with a weight ratio 1:1 and polymer concentration is 15 g/l. A spin-coating speed of 800 rpm yielded blend films with thickness between 80–90 nm. The blend films were annealed at 130 °C for 7 min on a hotplate before transferring to a vacuum evaporator inside a nitrogen purified glove box. Finally, a 1 nm LiF layer and an 80 nm aluminium layer were subsequently evaporated through a shadow mask making devices with active areas of ~11 $mm^2$.

*Device characterization*: Device measurements were conducted under purified nitrogen. A Keithley 2400 was used as a source-meter to measure current density vs. voltage (J-V) curves under AM 1.5 simulated illumination with 100 $mW/cm^2$ intensity. The intensity was calibrated with an NREL certified Si reference solar cell. A $\lambda = 632$ nm laser was used with a set of neutral density filters for light intensity J-V measurements where light intensities were recorded with a calibrated Si detector. Illumination for incident photon to current efficiency (IPCE) measurements was done with a chopped monochromatic beam where the signal under short-circuit conditions was measured with a lock-in amplifier. A calibrated Si detector was used to measure the light intensity.

*Grazing Incidence Wide-Angle X-ray Scattering (GIWAXS)*: GIWAXS measurements were performed at beamline 7.3.3 of Advanced Light Source.[56] Samples were prepared using identical blend solutions as those used in devices on a PSS pre-coated Si substrate. The 10 keV X-ray beam was incident at a grazing angle of 0.14°, which maximized the scattering intensity from the samples. The scattered intensity was detected with a Dectris Pilatus 1M photon counting detector.

*Resonant & Polarized Soft X-ray Scattering (R-SoXS & P-SoXS)*: R-SoXS transmission measurements were performed at beamline 11.0.1.2 at the Advanced Light Source (ALS).[57] Samples for R-SoXS measurements were first prepared on a PSS modified Si substrate under the same conditions as those used for device fabrication, and then transferred to a 1 mm × 1 mm, 100 nm thick Si3N4 membrane supported by a 5 mm × 5 mm, 200 μm thick Si frame (Norcada Inc.). 2-D scattering patterns were collected on an in-vacuum CCD camera (Princeton Instrument PI-MTE).

*Scanning Transmission X-ray Microscopy*: STXM measurements were performed at beamline 5.3.2.2 of the Advanced Light Source (ALS).[58] The TEM grid-supported films were mounted in the sample chamber, which was evacuated to 0.3 mbar and subsequently refilled with 1/3 atm of helium. The intensity of the focused X-ray beam transmitted through the film was recorded using a scintillator and photomultiplier tube and measured as a function of energy and position.

## Supporting Information

Supporting Information is available from the Wiley Online Library or from the author.

## Acknowledgements

X-ray characterization, device fabrication and device measurements by NCSU supported by the U.S. Department of Energy, Office of Science, Basic Energy Science, Division of Materials Science and Engineering under Contract DE-FG02-98ER45737. X-ray data was acquired at beamlines 11.0.1.2, 7.3.3, and 5.3.2.2. at the Advanced Light Source, which is supported by the Director, Office of Science, Office of Basic Energy Sciences, of the U.S. Department of Energy under Contract No. DE-AC02-05CH11231. Synthesis at South China University and Technology was funded by the Natural Science Foundation of China (No. 21125419). The authors also thank Yingchi Liu and Abay Gadisa for assistance with device measurements, A. L. D Kilcoyne and C. Wang for help with the data acquisition at the ALS.

Received: November 8, 2012
Revised: January 10, 2013
Published online: March 15, 2013

[1] V. Shrotriya, *Nat. Photon.* **2009**, *3*, 447–449.
[2] G. Li, R. Zhu, Y. Yang, *Nat. Photon.* **2012**, *6*, 153–161.
[3] G. Li, V. Shrotriya, J. Huang, Y. Yao, T. Moriarty, K. Emery, Y. Yang, *Nat. Mater.* **2005**, *4*, 864–868.
[4] L. Dou, J. You, J. Yang, C.-C. Chen, Y. He, S. Murase, T. Moriarty, K. Emery, G. Li, Y. Yang, *Nat. Photon.* **2012**, *6*, 180–185.

[5] Z. He, C. Zhong, S. Su, M. Xu, H. Wu, Y. Cao, *Nat. Photon.* **2012**, *6*, 591–595.
[6] T. L. Benanti, D. Venkataraman, *Photosynth. Res.* **2006**, *87*, 73–81.
[7] N. D. Treat, M. Brady, G. Smith, M. F. Toney, E. J. Kramer, C. J. Hawker, M. L. Chabinyc, *Adv. Energy Mater.* **2011**, *1*, 82–89.
[8] B. A. Collins, E. Gann, L. Guignard, X. He, C. R. McNeill, H. Ade, *J. Phys. Chem. Lett.* **2010**, *1*, 3160–3166.
[9] W. Yin, M. Dadmun, *ACS Nano* **2011**, *5*, 4756–4768.
[10] B. Watts, W. J. Belcher, L. Thomsen, H. Ade, P. C. Dastoor, *Macromolecules* **2009**, *42*, 8392–8397.
[11] B. A. Collins, J. R. Tumbleston, H. Ade, *J. Phys. Chem. Lett.* **2011**, *2*, 3135–3145.
[12] D. Chen, A. Nakahara, D. Wei, D. Nordlund, T. P. Russell, *Nano Lett.* **2011**, *11*, 561–7.
[13] N. D. Treat, A. Varotto, C. J. Takacs, N. Batara, M. Al-hashimi, M. J. Heeney, A. J. Heeger, F. Wudl, C. J. Hawker, M. L. Chabinyc, *J. Am. Chem. Soc.* **2012**, *134*, 15869–15879.
[14] A. Guilbert, L. Reynolds, A. Bruno, A. MacLachlan, S. P. King, M. Faist, E. Pires, J. E. Macdonald, N. Stingelin, S. Haque, J. Nelson, *ACS Nano* **2012**, *6*, 3868–75.
[15] F. C. Jamieson, E. B. Domingo, T. McCarthy-Ward, M. Heeney, N. Stingelin, J. R. Durrant, *Chem. Sci.* **2012**, *3*, 485.
[16] A. Herzing, L. J. Richter, I. M. Anderson, *J. Phys. Chem. C* **2010**, *114*, 17501–17508.
[17] M. Pfannmöller, H. Flügge, G. Benner, I. Wacker, C. Sommer, M. Hanselmann, S. Schmale, H. Schmidt, F. Hamprecht, T. Rabe, W. Kowalsky, R. R. Schröder, *Nano Lett.* **2011**, *11*, 3099–107.
[18] D. R. Kozub, K. Vakhshouri, L. M. Orme, C. Wang, A. Hexemer, E. D. Gomez, *Macromolecules* **2011**, *44*, 5722–5726.
[19] C. R. McNeill, *J. Polym. Sci. B Polym. Phys.* **2011**, *49*, 909–919.
[20] C. R. McNeill, H. Ade, *J. Mater. Chem. C* **2013**, *1*, 187–201.
[21] B. A. Collins, H. Ade, *J. Electron Spectrosc. Relat. Phenom.* **2012**, *185*, 119–128.
[22] L. Yang, J. R. Tumbleston, H. Zhou, H. Ade, W. You, *Energy Environ. Sci.* **2013**, *6*, 316–326.
[23] B. A. Collins, Z. Li, J. R. Tumbleston, E. Gann, C. R. McNeill, H. Ade, *Adv. Energy Mater.* **2012**, *3*, 65–74.
[24] S. Albrecht, W. Schindler, J. Kurpiers, J. Kniepert, J. C. Blakesley, I. Dumsch, S. Allard, K. Fostiropoulos, U. Scherf, D. Neher, *J. Phys. Chem. Lett.* **2012**, *3*, 640–645.
[25] B. P. Lyons, N. Clarke, C. Groves, *Energy Environ. Sci.* **2012**, *5*, 7657.
[26] J. A. Bartelt, Z. M. Beiley, E. T. Hoke, W. R. Mateker, J. D. Douglas, B. A. Collins, J. R. Tumbleston, K. R. Graham, A. Amassian, H. Ade, J. M. J. Frechet, M. F. Toney, M. D. McGehee, *Adv. Energy Mater.* **2013**, *3*, 364–374.
[27] H. Yan, S. Swaraj, C. Wang, I. Hwang, N. C. Greenham, C. Groves, H. Ade, C. R. McNeill, *Adv. Funct. Mater.* **2010**, *20*, 4329–4337.
[28] L. Ye, S. Zhang, W. Ma, B. Fan, X. Guo, Y. Huang, H. Ade, J. Hou, *Adv. Mater.* **2012**, *24*, 6335–6341.
[29] B. A. Collins, J. E. Cochran, H. Yan, E. Gann, C. Hub, R. Fink, C. Wang, T. Schuettfort, C. R. McNeill, M. L. Chabinyc, H. Ade, *Nat. Mater.* **2012**, *11*, 536–543.
[30] B. P. Rand, D. Cheyns, K. Vasseur, N. C. Giebink, S. Mothy, Y. Yi, V. Coropceanu, D. Beljonne, J. Cornil, J.-L. Brédas, J. Genoe, *Adv. Funct. Mater.* **2012**, *22*, 2987–2995.
[31] Y. Yi, V. Coropceanu, J.-L. Brédas, *J. Am. Chem. Soc.* **2009**, *131*, 15777–15783.
[32] A. Ojala, A. Petersen, A. Fuchs, R. Lovrincic, C. Pölking, J. Trollmann, J. Hwang, C. Lennartz, H. Reichelt, H. W. Höffken, A. Pucci, P. Erk, T. Kirchartz, F. Würthner, *Adv. Funct. Mater.* **2012**, *22*, 86–96.
[33] M. Wang, X. Hu, P. Liu, W. Li, X. Gong, F. Huang, Y. Cao, *J. Am. Chem. Soc.* **2011**, *133*, 9638–9641.
[34] D. Chen, F. Liu, C. Wang, A. Nakahara, T. P. Russell, *Nano Lett.* **2011**, *11*, 2071–8.
[35] H. Yan, B. A. Collins, E. Gann, C. Wang, H. Ade, *ACS Nano* **2012**, *6*, 677–688.
[36] S. Swaraj, C. Wang, H. Yan, B. Watts, J. Lüning, C. R. McNeill, H. Ade, *Nano Lett.* **2010**, *10*, 2863–9.
[37] B. A. Collins, Z. Li, C. R. McNeill, H. Ade, *Macromolecules* **2011**, *44*, 9747–9751.
[38] T. Yang, M. Wang, C. Duan, X. Hu, L. Huang, J. Peng, F. Huang, X. Gong, *Energy Environ. Sci.* **2012**, *5*, 8208–8214.
[39] V. D. Mihailetchi, H. X. Xie, B. de Boer, L. J. A. Koster, P. W. M. Blom, *Adv. Funct. Mater.* **2006**, *16*, 699–708.
[40] J. R. Tumbleston, Y. Liu, E. T. Samulski, R. Lopez, *Adv. Energy Mater.* **2012**, *5*, 477–486.
[41] V. Mihailetchi, J. Wildeman, P. Blom, *Phys. Rev. Lett.* **2005**, *94*, 1–4.
[42] T. Coffey, S. G. Urquhart, H. Ade, *J. Electron Spectrosc. Relat. Phenom.* **2002**, *122*, 65–78.
[43] A. M. Ballantyne, T. A. M. Ferenczi, M. Campoy-Quiles, T. M. Clarke, A. Maurano, K. H. Wong, W. Zhang, N. Stingelin-Stutzmann, J.-S. Kim, D. D. C. Bradley, J. R. Durrant, I. McCulloch, M. Heeney, J. Nelson, S. Tierney, W. Duffy, C. Mueller, P. Smith, *Macromolecules* **2010**, *43*, 1169–1174.
[44] S. Albrecht, S. Janietz, W. Schindler, J. Frisch, J. Kurpiers, J. Kniepert, S. Inal, P. Pingel, K. Fostiropoulos, N. Koch, D. Neher, *J. Am. Chem. Soc.* **2012**, *134*, 14932–44.
[45] C. Deibel, V. Dyakonov, *IEEE Journal of Selected Topics in Quantum Electronics* **2010**, *16*, 1517–1527.
[46] R. R. Lunt, N. C. Giebink, A. A. Belak, J. B. Benziger, S. R. Forrest, *J. Appl. Phys.* **2009**, *105*, 053711.
[47] P. E. Shaw, A. Ruseckas, I. D. W. Samuel, *Adv. Mater.* **2008**, *20*, 3516–3520.
[48] M. R. Hammond, R. J. Kline, A. A. Herzing, L. J. Richter, D. S. Germack, H.-W. Ro, C. L. Soles, D. A. Fischer, T. Xu, L. Yu, M. F. Toney, D. M. Delongchamp, *ACS Nano* **2011**, *5*, 8248–57.
[49] I. Osaka, M. Shimawaki, H. Mori, I. Doi, E. Miyazaki, T. Koganezawa, K. Takimiya, *J. Am. Chem. Soc.* **2012**, *134*, 5425.
[50] J. H. Park, J.-I. Park, D. H. Kim, J.-H. Kim, J. S. Kim, J. H. Lee, M. Sim, S. Y. Lee, K. Cho, *J. Mater. Chem.* **2010**, *20*, 5860.
[51] H. Cha, J. W. Park, D. S. Chung, T. K. An, Y.-H. Kim, S.-K. Kwon, C. E. Park, *J. Mater. Chem.* **2012**, *22*, 15141.
[52] J. Rivnay, R. Noriega, R. Kline, A. Salleo, M. Toney, *Phys. Rev. B* **2011**, *84*, 1–20.
[53] J. T. Rogers, K. Schmidt, M. F. Toney, E. J. Kramer, G. C. Bazan, *Adv. Mater.* **2011**, *23*, 2284–8.
[54] W. Chen, T. Xu, F. He, W. Wang, C. Wang, J. Strzalka, Y. Liu, J. Wen, D. J. Miller, J. Chen, K. Hong, L. Yu, S. B. Darling, *Nano Lett.* **2011**, *11*, 3707–13.
[55] X. He, B. A. Collins, B. Watts, H. Ade, C. R. McNeill, *Small* **2012**, *8*, 1920–7.
[56] A. Hexemer, W. Bras, J. Glossinger, E. Schaible, E. Gann, R. Kirian, A. MacDowell, M. Church, B. Rude, H. Padmore, *J. Phys. Conf. Ser.* **2010**, *247*, 012007.
[57] E. Gann, A. T. Young, B. A. Collins, H. Yan, J. Nasiatka, H. A. Padmore, H. Ade, A. Hexemer, C. Wang, *Rev. Sci. Instrum.* **2012**, *83*, 045110.
[58] A. L. D. Kilcoyne, T. Tyliszczak, W. F. Steele, S. Fakra, P. Hitchcock, K. Franck, E. Anderson, B. Harteneck, E. G. Rightor, G. E. Mitchell, A. P. Hitchcock, L. Yang, T. Warwick, H. Ade, *J. Synchrotron Rad.* **2003**, *10*, 125–136.